J Mater Sci (2009) 44:2408–2418
DOI 10.1007/s10853-009-3308-z

Forming contacts and grain boundaries between MgO nanoparticles

Julia Deneen Nowak · C. Barry Carter

Received: 4 October 2008 / Accepted: 30 January 2009 / Published online: 26 February 2009

Abstract The present article is concerned with how nanoparticles join: it considers MgO nano-cubes as a model, well-defined system. The development of grain boundaries (GBs) between cube particles has been re-examined using MgO smoke. In addition to the face-to-face contact which leads to the well-known low-$\sum$ twist GBs, interactions are also found which initially involve point-to-face contact, edge-to-face contact, or contacts along the cube edges. It is proposed here that the point contact lead to a line contact through the requirement to balance charges, and rotation about such a *line of contact leads to formation of the interface*, i.e., the grain boundary. The atoms along the edges have lower coordination than the atoms in the bulk, which may contribute to the edge–edge and edge-face boundary formation. The inherently small size of nanoparticles makes transmission electron microscopy (TEM) an invaluable technique for characterizing the contacts between them without modifying them in any way. The present study uses TEM to characterize the types of boundaries formed, discusses the boundary structures, and considers how the particle morphology may determine the formation of low-$\sum$ GBs.

Julia Deneen Nowak and C. Barry Carter were previously at Department of Chemical Engineering and Materials Science, University of Minnesota, 421 Washington Avenue SE, Minneapolis, MN, 55455, USA.

J. D. Nowak
Hysitron, Inc., 10025 Valley View Rd., Minneapolis, MN 55344, USA

C. B. Carter (✉)
Department of Chemical, Materials & Biomolecular Engineering, University of Connecticut, 191 Auditorium Road, Storrs, CT 06269, USA
e-mail: cbcarter@engr.uconn.edu

Introduction

Nanotechnology is quite well developed but the underlying science is still being explored. Nanoparticles, in particular have widespread uses (e.g., [1–3]) but their usefulness is often limited by their tendency to agglomerate and grow into larger entities (e.g., [4]). Magnesium oxide (MgO) has been of interest for decades because its properties make it useful in a broad range of applications [5]. Bulk MgO is regularly used as a substrate material for the growth of thin films due to the ease with which it can be cleaved or polished to provide atomically flat (100) surfaces [6–9]. MgO also has a high thermal resistivity (42 Wm^{-1} K^{-1}) and a very high melting point (2800 °C). These two properties are used in many high-temperature applications such as refractory brick, crucibles, and furnace linings. Additionally, the low dielectric constant (9.65 at 1 MHz) of MgO makes it useful as a substrate material for high-*Tc* superconductor applications, and its low refractive index (1.735) is ideal for optical confinement in ferroelectric/MgO/semiconductor waveguide structures [10]. MgO thin films are used in waveguide applications because they can be grown in preferred orientations relatively easily and the structure is lattice-matched to a number of materials [10]. For example, perovskite thin films are difficult to grow directly on Si, but MgO is lattice-matched with both materials and can be used as a buffer layer [10]. Also, thin films of MgO have been proposed for use as protective coatings on the phosphor screens in plasma display panels [11] due to their anti-sputtering properties, high

transmittance, and secondary-electron emission characteristics [12–14].

The ionic charge is not compensated at the corners, edges, or surfaces of cubic MgO particles. It is this property that has made fine-grain MgO powders historically useful in antacids. Today, the large fraction of low-coordinated edge and corner atoms in MgO nanoparticles also makes the particles particularly effective as reactive adsorbents; they react with organophosphorus compounds by dissociative chemisorption to create nontoxic products, making MgO nanoparticles effective in the decontamination of agents that could be used in chemical warfare [15, 16]. MgO nanoparticles are also found to be effective in reducing chlorofluorocarbons. For example, MgO can be successfully reacted with CF_2Cl_2 to form MgF_2, CCl_4, and CO_2 [17].

Background

MgO is a rocksalt-structure material in which the bonds exhibit a large ionic character (~73%). The structure of MgO can be described as an FCC lattice with a two-atom basis consisting of O^{2-} anions at the (000) positions and Mg^{2+} cations at the (½ ½ ½) positions. The lattice parameter is 0.421 nm. The structure is shown schematically in Fig. 1. In its bulk form, MgO is generally considered to be an inert oxide, though this is not true for nanoscale MgO. Atoms at surfaces, edges and corner have a lower coordination than do those in the bulk. In nanoscale MgO, atoms at these locations provide a high density of catalytically active sites. The fraction of atoms in such sites increases with decreasing particle size. This phenomenon makes the normally inert MgO useful in the form of nanoparticles as a heterogeneous basic catalyst [18–20]. These catalytic applications are particularly relevant to the present study since they result from the fact that the ionic charge is not locally balanced at corners, edges, or faces of an MgO cube.

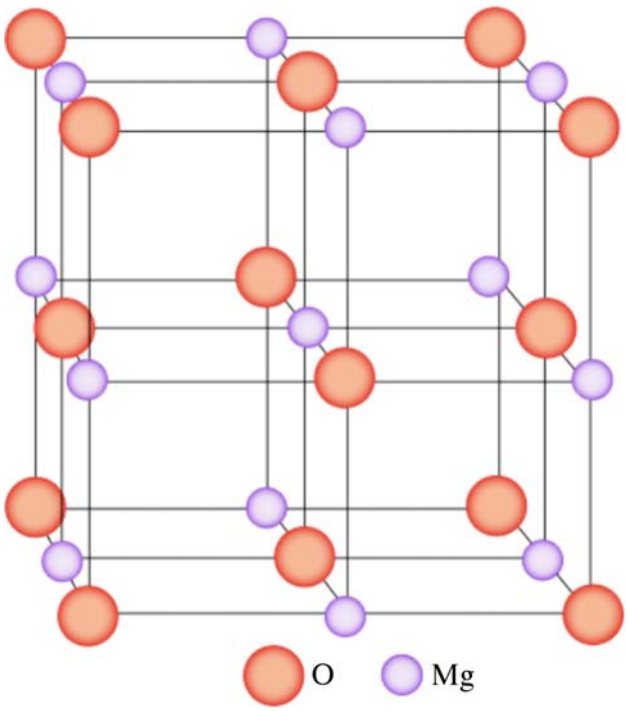

Fig. 1 The FCC unit cell of MgO

Nanoscale structures of MgO can be produced by a variety of methods, which in turn produce a variety of morphologies [21–24]. Polyhedral shells, nanotubes, nanocubes, and nanowires have been produced by thermal evaporation [22]. Nanorods have been grown through carbothermal reduction of MgO followed by subsequent nucleation and reoxidation [24], while nanobelts have been grown by the decomposition and oxidation of Mg_3N_2 [21]. Further research is needed to understand these different formation processes [25].

Incorporation of MgO nanoparticles in applications requires an understanding not only of the properties of individual particles, but also of how the nanoparticles interact with, and bond to, one another. The large fraction of surface atoms in MgO nanocubes, which see different coordination to those in the interior, must also affect the formation of boundaries in the largely ionic crystals. Conversely, differently shaped MgO particles can be expected to behave very differently.

The nanoparticles present in MgO smoke are particularly well suited for studies using the TEM because the small particles are electron transparent and can be directly examined in the TEM [26]. The process of burning magnesium metal to produce small cubes of MgO that were then characterized in the TEM was described by Heidenreich in 1942 [27]. The statistical occurrence of twist boundaries between MgO smoke particles was examined three decades later by Chaudhari and Matthews [28, 29], who considered the geometry of boundary formation using the coincident-site lattice (CSL) notation [28–30]. Subsequent studies of MgO smoke have investigated various properties of the smoke particles, including the size distribution [31], growth kinetics [32], optical properties [33], and surface features [34, 35]. However, the role of the cube corners and edges in boundary formation has largely been ignored. The present study uses TEM to characterize the various types of boundaries found in MgO smoke particles.

Experimental

TEM samples were prepared by burning small pieces of Mg metal in air. The reaction $2Mg + O_2 = 2MgO$ produces 'smoke' consisting of nanoparticles of MgO. The smoke particles were then caught by suspending a TEM grid with a

thin support film (in this study amorphous carbon) in the smoke plume. The particles produced are usually cubes with (100) faces and edge lengths on the order of a few tens of nanometers. Fresh samples were deposited directly prior to TEM sessions to avoid prolonged exposure to humidity, which is known to cause surface hydroxylation [35]. The particles were characterized using a Tecnai G2 F30 TEM operated at 300 kV. Since the support film was held some distance (up to 24 inches) away from the hot zone (the flame), it can be assumed that the particles have achieved their final shape before being caught on the support film. Studies are in progress using more robust substrates to catch the particles at an earlier stage in their growth [36].

Results

A TEM image of a typical distribution of MgO nanocubes is shown in Fig. 2; cubes that are much smaller ($\sim$20 nm edge length) can be seen in the subsequent images. It is generally assumed that the MgO particles nucleate as cubes and then grow, retaining the cubic shape; the shape of these small cubes is consistent with this assumption. The 50-100 nm cubes typically agglomerate in small clusters, predominately by forming three types of boundaries which are here referred to as point contacts, line contacts, and face contacts. It is particularly relevant that no moiré fringes are present in this image.

Point contact

Point contacts are uncommon but are occasionally observed, as illustrated in Fig. 3. The corner of one grain is in contact with the face of a second grain and shows bend contours indicating a deformation of the corner region.

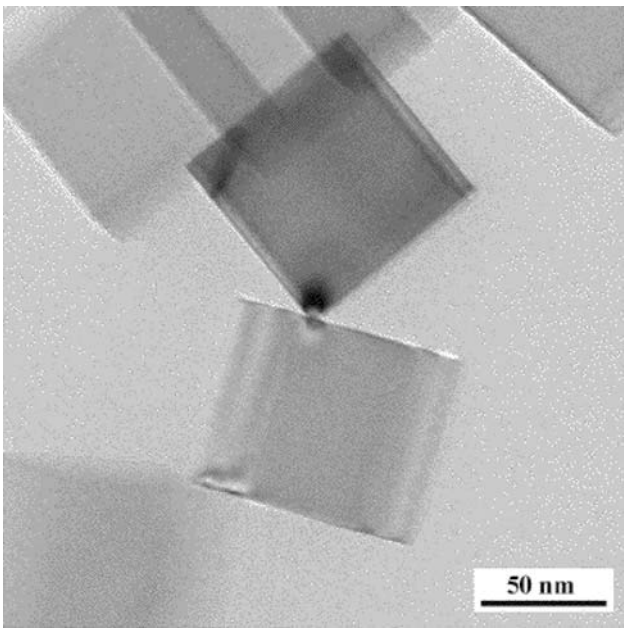

Fig. 3 A point contact in MgO

Line contact

Occasionally two cubes appear to contact one another exactly along one common edge, as shown in Fig. 4. The two particles in this figure are in nearly identical orientations with respect to the electron beam, as indicated by their thickness fringes. (Examples are identified by arrows

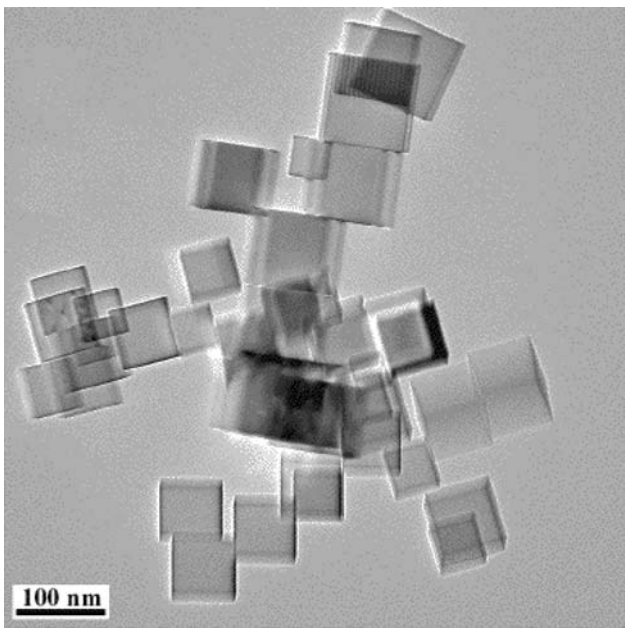

Fig. 2 Bright-field TEM image of a cluster of MgO smoke particles

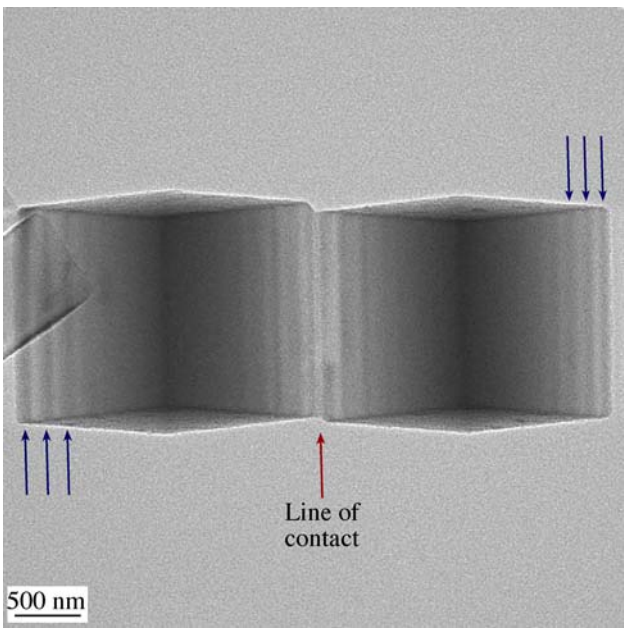

Fig. 4 An edge–edge boundary between two MgO cubes

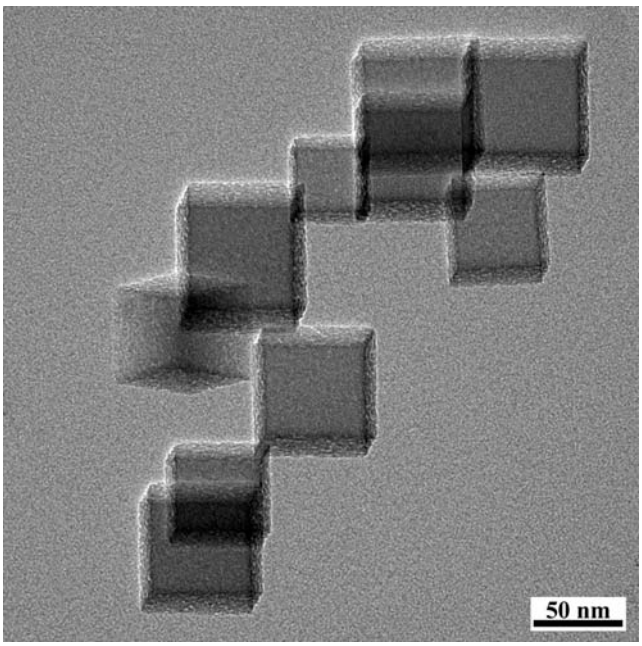

Fig. 5 Edge–edge boundaries with >1 neighbor

in Fig. 4.) The particles are also nearly identical in size and the fringes are symmetric on either side of the line of contact. A single particle can also form line contacts (including edge–edge boundaries as a special case) with more than one particle. Figure 5 shows a situation where several individual cubes forms line contacts with two adjacent cubes. (The surfaces of these cubes show the effect of beam damage due to the electron beam but this does not, of course, affect the relative orientations.)

Face contact

The large majority of the boundaries are between particles which contact one another such that there is little or no rotation of their shared (100) faces about the common ⟨100⟩ face normal. In a variation on such a boundary, the particles are again in contact across their (100) faces, but are now rotated about the common ⟨100⟩ face normal. Assuming the grains are in intimate contact, these GBs must be essentially pure twist in character. The rotation can be determined from the image or from the diffraction

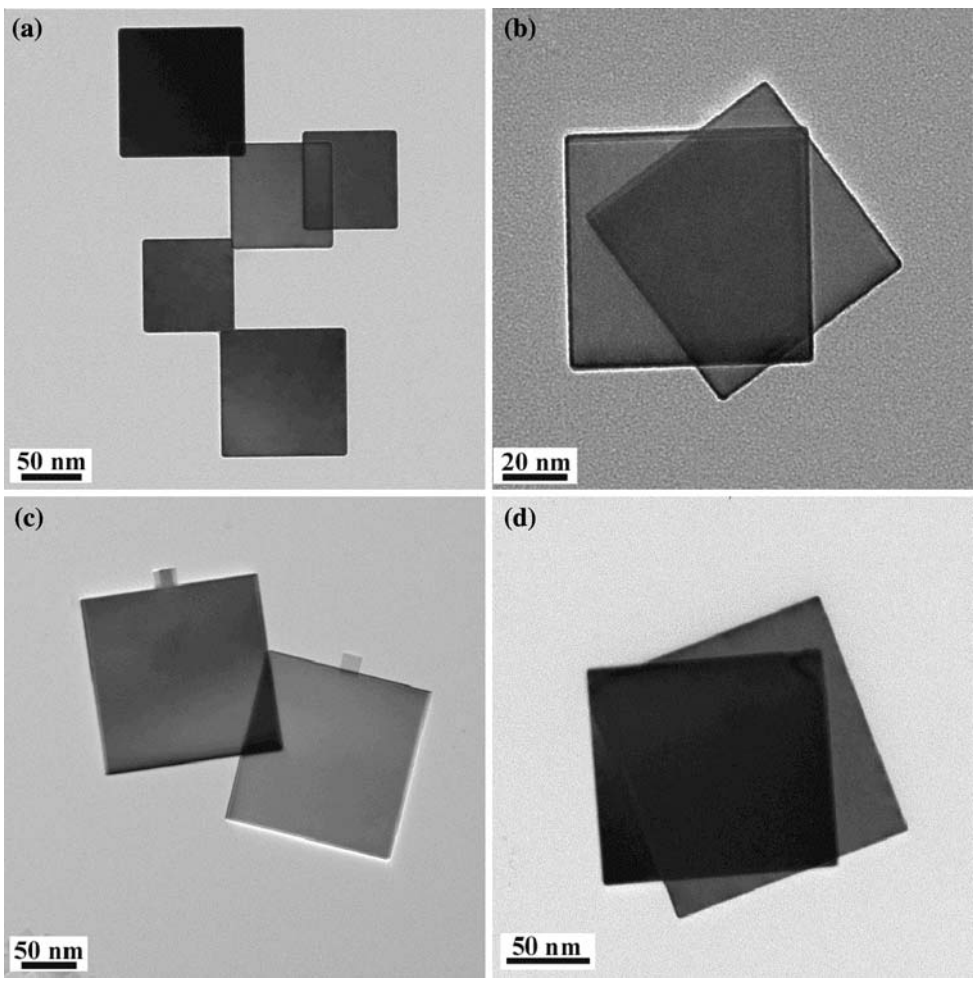

Fig. 6 TEM images of boundaries between MgO smoke particles with **a** no rotation, **b** 36.9°, **c** 22.6°, and **d** 16.3°

pattern. Figure 6 illustrates two types of twist GBs. Figure 6a shows the most common type of GB in which the angle of rotation is 0°. The GBs shown in Fig. 6b, c, and d have misorientation angles of 36.9°, 22.6°, and 16.3° respectively. All the MgO particles were perfect crystals; none were found to contain bulk lattice defects. The lack of moiré fringes in Fig. 2 implies that there are no small rotations away from near-perfect alignment in the case of the $\sum = 1$ GBs.

Figure 7a shows a dark-field TEM image and the corresponding SAD pattern of two smoke particles that have been oriented such that the GB between them is edge-on. A close inspection of the SAD pattern, shown in Fig. 7b, indicates that the two particles are not in identical orientations with respect to the electron beam. The contrast features (the white dashes along the arrowed GB) seen in Fig. 7a are actually edge dislocations with the usual $\frac{1}{2}\langle 110\rangle$ Burgers vectors.

A few particles are found that have clearly grown together as illustrated in Fig. 8 where two rectangular particles join in perfect alignment along a plane that is not {001}. This intergrowth indicates that the particles can actually join together in the hot plume before they finished

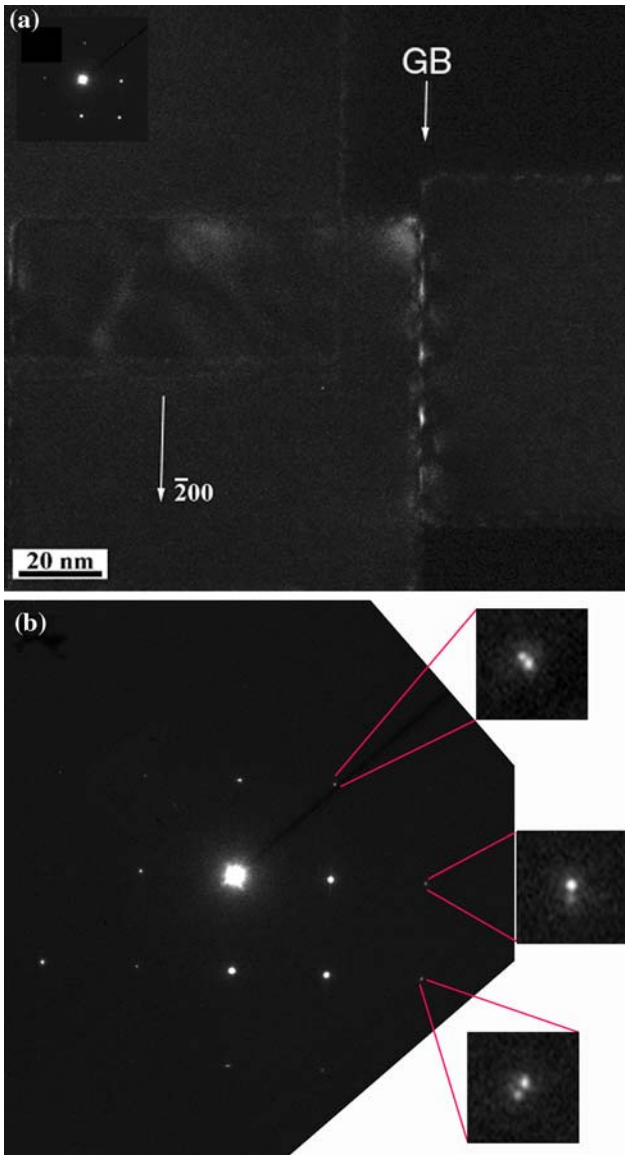

Fig. 7 Small-angle tilt boundary in MgO smoke. **a** The two cubes are oriented such that the boundary is edge-on. **b** SAD pattern shown in A with 220, 040, and $\bar{2}40$ reflections (from top to bottom) shown at higher magnification

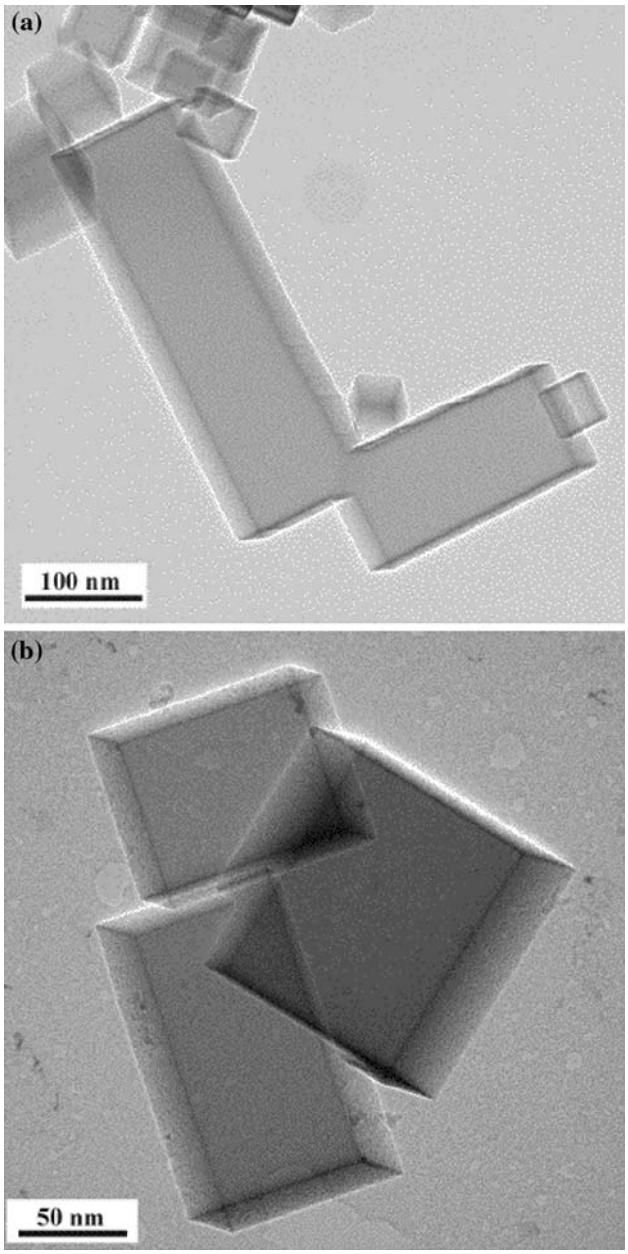

Fig. 8 Growth boundaries in MgO smoke particles. Unlike twist boundaries, these particles have grown together. In (**a**) a single particle has grown with two elongated branches. In (**b**) particles have intergrown

growing. The rectangular shape of such particles may also result from early particle coalescence and growth, but there is presently no direct evidence for this process.

Discussion

The contacts between MgO particles occur while the particles are in the smoke plume and are hot; the particles move as a result of convection currents and Brownian motion [28, 29]. As the particles develop in the smoke plume one will most likely first contact another at a point; the point contact can be made when the corner of one cube contacts a second cube, or when the edges of two cubes contact at a single point. The particles can then rotate with respect to one another until they reach an orientation for which the contact energy is sufficiently low. Experimentally, contacts are observed at cube corners, along cube edges, and between cube faces. The observation of the bend contours has been explained [37, 38] by the fact that the particles elastically deform at the corner to produce a small contact area thus lowering the total surface energy. In MgO this process might be limited by charge repulsion but clearly it does take place. Throughout the following discussion, no assumptions are made as to relaxations at, or reconstruction of, the surface of the nanoparticles. The charges at corners and edges are considered but no assumptions are made as to the actual distribution of charge during processing. It is clear, however, that the joined particles were at high temperature when they may contact, but how long they remained at this temperature after they had made contact is not known. This latter consideration would be a factor in any subsequent rearrangement or rotation.

The large surface-to-volume ratio of small particles can have a notable effect on contact formation. For MgO, the atoms at the faces, corners, and edges of the cube see different coordination to those in the bulk. In the bulk each ion has six equidistant, oppositely charged, nearest neighbors, while surface atoms have only five neighbors, edge atoms have only four neighbors, and corner atoms have only three neighbors. In small particles these atoms can constitute a large fraction of the total number of atoms. For example, in a 5 nm MgO nanocube there are approximately 13,400 atoms. Of these atoms, nearly 6,400 are surface atoms with five nearest neighbors, 420 are edge atoms with four nearest neighbors, and 8 are corner atoms with only three nearest neighbors. Thus, approximately 50% of the atoms in the particle have coordination that is different from the 'bulk'. It is proposed that these low-coordinated surface atoms can play a significant role in the nature of the contacts formed between the particles.

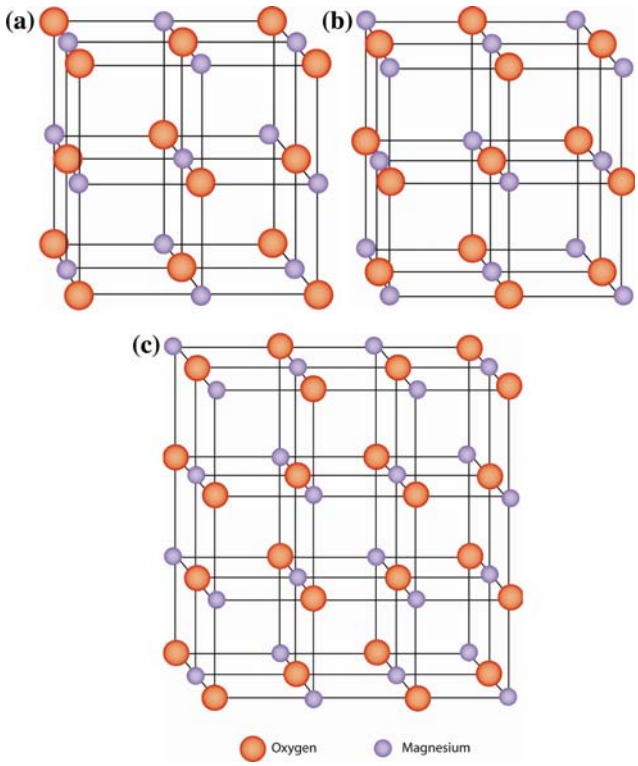

Fig. 9 The net charge of a cube of MgO depends on which ions are present at the cube corners. In (**a**) the net charge is −2, in (**b**) it is +2, and in (**c**) the net charge is zero

Schematics of nanoparticles are shown in Fig. 9. The coordination of the corner atoms and the net charge of the MgO cube may also play a role in the specific arrangement of contacting cubes. For a perfect cube of MgO, the net charge can be −2, +2, or 0 as shown in Fig. 9. If all of the corner atoms are O^{2-} there will be one more O^{2-} ion than there are Mg^{2+} ions and the net charge will be −2. Similarly, if all of the corner atoms are Mg^{2+} the net charge will be +2. Only if four corner atoms are Mg^{2+} and four are O^{2-} will the net charge be 0. When contact occurs between two cubes, the charge on a corner atom can be balanced if that atom contacts the corner (of opposite charge) or the edge of the other cube.

Point contact

When contacts form between particles, the particles will orient themselves in a manner that will minimize the energy of the contact region. With the large fraction of under-coordinated sites on the surfaces and edges of MgO nanocubes, these contacts generally involve specific arrangements involving the cube edges and faces. If the corner of one cube contacts the face of another, the particles will likely rotate in the smoke to a configuration with lower interfacial energy. However, if there is not sufficient

time or energy to form a larger area of contact, point contacts can form. Point contacts are uncommon but are occasionally observed (Fig. 3). Since it is energetically more favorable for the particles to be in contact over an area than at a point, the contact area usually automatically increases and in doing so creates a stress field at the contact [37]. The stress field is balanced by a compressive stress at the center of the contact and a tensile stress at the exterior [38–41]. The strain-contrast contour is visible in Fig. 3, most notably in the corner contacting the face. This type of strain contrast is also observed in contacting nanospheres [42] and has been extensively described and matched with computed images, by Tholen. (The topic is well reviewed in [37].) Of course, after contact the point is no longer a point but instead is a small contact area. This small area cannot be imaged in the TEM and is thus best modeled and simulated images matched to the observed ones [37]. To test the 3D nature of the strain, the sample can be, and was, tilted and the changes in the bend contours observed.

Line contacts

Because of the ionic nature of MgO, and the low coordination of the atoms along the cube edges, the formation of a line boundary (or an edge–edge boundary) can serve to lower the interfacial energy. The atoms along the cube edge, which consist of alternating Mg^{2+} and O^{2-} ions, possess a lower coordination than those in the bulk or those on the (100) surfaces. It is possible that, in the smoke, two particles may come into contact such that their edges directly form a contact without any rotation, though this is unlikely. However, if a point contact is formed between two cube edges, the particles can then rotate about this point until the edges of the two cubes are contacting along their length. For two cubes contacting in this manner, an a/2 translation along the edge of two identical cubes could completely satisfy the nearest neighbor bonding. The geometry of these line contacts will be discussed using the $\sum$ notation described below.

Small-angle GB formation

Small-angle GBs form when two crystals are oriented with a slight misorientation, which can be accommodated by a network of dislocations. The number and spacing of the dislocations is determined by the angle of misorientation. This relationship is given by the simplified Frank formula (see [5]):

$$\sin\frac{\theta}{2} = \frac{b}{2D} \tag{1}$$

where D is the dislocation spacing, b is the burgers vector, and θ is the angle of misorientation.

The dark-field TEM image and the corresponding SAD pattern of two smoke particles in Fig. 6 confirms that both crystals are being viewed close to the [001] direction, but that there is a small rotation about this axis which results in two spots for each reflection (one from each crystal). This rotation indicates that the GB is not a small-angle twist GB. Since the axis of rotation lies in the GB plane, the interface is a small-angle tilt GB and the misorientation is accommodated by edge dislocations, which are visible as bright spots along the boundary. The angle of tilt can be measured from the diffraction pattern, and in this case is approximately 1°. The dislocations, as measured from the image, are evenly spaced approximately 16 nm apart. This value is consistent with the 17 nm spacing calculated using the tilt angle measured from the SAD pattern and Eq. 1.

The misorientation at small-angle tilt GBs is accommodated by a network of edge lattice dislocations; in the case of two contacting crystals, these dislocations can originate from surface steps on the nearly flat (001) surface, shown schematically in Fig. 10. Since the dislocations in Fig. 7a are visible, the burgers vector must satisfy the condition $\mathbf{g} \cdot \mathbf{b} \neq 0$. The image was formed using the $\bar{2}00$ reflection, as indicated by the arrow in the figure. For $\mathbf{g} = \bar{2}00$, a number of different Burgers vectors are possible, as summarized in Table 1. For $\mathbf{b} = \frac{1}{2}\langle 110\rangle$, the Burgers vector lies in the GB plane, and for $\mathbf{b} = \frac{1}{2}\langle 110\rangle$, it

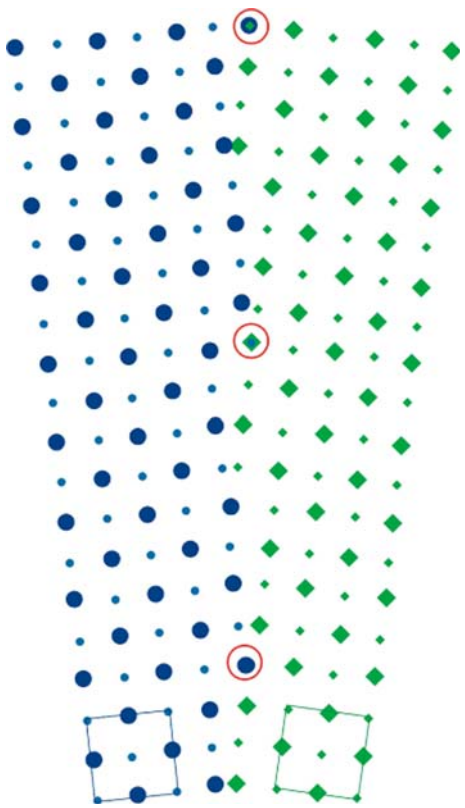

Fig. 10 Ion matching along a line formed by a line contact

Table 1 All possible burgers vectors for the dislocations in the particles shown in Fig. 7a, where $\mathbf{g} = \bar{2}00$ and $\mathbf{b} = 002$

b	**g · b**	Orientation with respect to boundary plane
$\frac{1}{2}[101]$	−1	In boundary plane
$\frac{1}{2}[10\bar{1}]$	−1	In boundary plane
$\frac{1}{2}[\bar{1}01]$	1	In boundary plane
$\frac{1}{2}[\bar{1}0\bar{1}]$	1	In boundary plane
$\frac{1}{2}[110]$	−1	45° out of boundary plane
$\frac{1}{2}[1\bar{1}0]$	−1	45° out of boundary plane
$\frac{1}{2}[\bar{1}10]$	1	45° out of boundary plane
$\frac{1}{2}[\bar{1}\bar{1}0]$	1	45° out of boundary plane
$\frac{1}{2}[011]$	0	Not a possible burgers vector
$\frac{1}{2}[01\bar{1}]$	0	Not a possible burgers vector
$\frac{1}{2}[0\bar{1}1]$	0	Not a possible burgers vector
$\frac{1}{2}[0\bar{1}\bar{1}]$	0	Not a possible burgers vector

is inclined 45° to the GB plane. The proposed dislocation structure in this GB is alternating ½[$\bar{1}$10] and ½[110], such that the net Burgers vector is [010] [43], which is perpendicular to the GB plane [44].

One important conclusion that can be drawn from this observation is that it gives definite proof that the cubes are in intimate contact. It is proposed that these two particles came into contact before the cubes had finished growing so that there were still steps on the surfaces.

High-angle GB formation

When two contacting crystals are misoriented by a rotation about a common axis, one or more lattice sites may be coincident across the GB plane. For an arbitrary angle of rotation it is unlikely that more than one site will be coincident, but for certain specific orientations a large fraction of the lattice points will coincide and the GB can form a special configuration. The coincident-site lattice (CSL) model is commonly used to describe these unique angles of misorientation between two crystals [30]. The GB configurations are described as $\Sigma = n$ boundaries where one in n lattice sites would be coincident if both grains forming the bicrystal were to be continued indefinitely. For example, Fig. 11 is a schematic of a $\Sigma = 5$ twist GB in which one crystal is blue (circle) and the other is green (diamond). One in five lattice sites is common between the two crystals, which is easily visualized in this schematic. The CSL model is only a geometric construction used to describe these types of GBs, though the frequency with which the GBs are found suggests that they are associated with a low energy [45]. GBs which can be described using the CSL model are found experimentally in oriented bicrystals [46, 47]; the existence of such GBs has been attributed to their having a low interfacial energy [48].

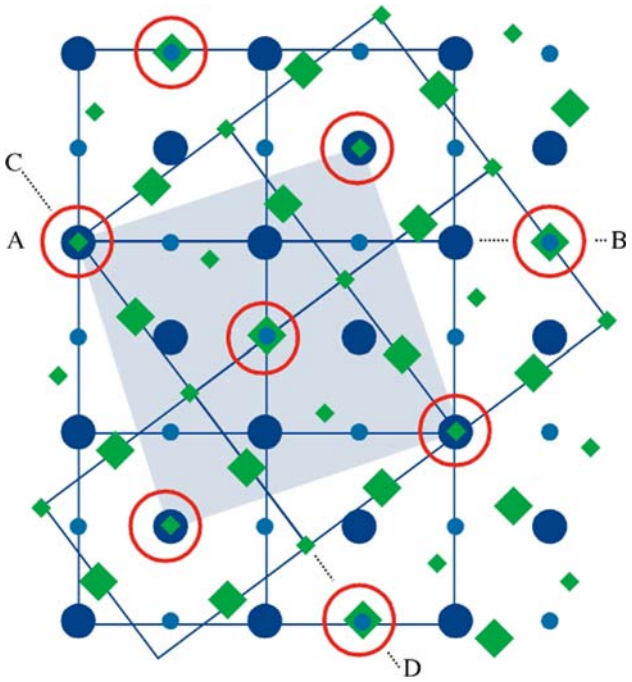

Fig. 11 Dislocation model of a small-angle tilt boundary

Evidence for this comes from the observation of secondary dislocations in high-angle GBs which preferentially rotate regions of a GB back into the exact $\sum = 5$ orientation.

The most common type of contact between MgO smoke particles is indeed observed when two the {001} faces of two particles are in contact, i.e., the particles are separated by a twist boundary. Such face-to-face boundaries are present in the image in Heidenreich's 1942 article on MgO smoke, but although the manuscript discusses some of the earliest observations of thickness fringes in MgO crystals, the boundaries themselves are not mentioned [27]. In the present study, when particles contact face-to-face, the two particles share a common (100) face but are usually not rotated about the ⟨100⟩ direction normal to this face. However, both twist and tilt about this contact can create other boundary configurations.

MgO has a number of predicted CSL {100} twist GBs. The most commonly observed orientations are GBs in which n, using the $\Sigma = n$ notation, is 5, 13, 17, or 25, though $\Sigma = 17$ GBs are only reported occasionally [28, 29, 49]. The $\Sigma = 5$, $\Sigma = 13$, and $\Sigma = 25$ GBs shown in Fig. 6b, c, and d have misorientation angles of 36.9°, 22.6°, and 16.3° respectively. Boundaries with these specific misorientations are observed with some frequency in the MgO smoke, which suggests that they are associated with a low energy. It is also noted that a study of the distribution of GBs in polycrystalline MgO has found that there is a preference for GBs with a boundary-plane normal that is in a ⟨100⟩ direction [50, 51] and that the $\sum = 5$ did indeed appear more frequently than expected from a random

distribution [50] and that there is a direct correlation with the presence of low-energy surfaces.

The large number of face-to-face boundaries observed in the MgO smoke is consistent with most of the cubes already having achieved their full size and cube shape before they come into contact. In the smoke, the cube particles probably initially contact at a point and then rotate about the contact until a minimum total energy is reached. The most likely type of point contact is formed when the corner of one cube contacts the face of a second cube. The particles can then rotate about the point contact until an edge of the first cube contacts the face of the second, forming a line contact; the cubes can then further rotate about this line to form a face-to-face contact. The difficulty in rotating one crystal after the GB has formed is that the screw dislocations that accommodate any misorientation must then glide (assuming that the two grains are in intimate contact) and dislocation glide in MgO is difficult.

Converting a line contact to a low-$\sum$ twist GB

An example of a line diagram is shown in Fig. 12. The special feature is the matching along this line. For example in Fig. 11, one in five of the large blue circles overlaps a small green diamond in the shaded unit cell of the GB (along AB or CD). It has often previously been proposed that low-$\sum$ CSL GBs have a lower energy than other GBs. Here it is proposed that lines of line contacts are configurations with particularly low energies. Such a line of contact might be further stabilized by slightly shifting the two edges or by forming a second line of contact with a third particle. (See e.g., Fig. 5.)

If the number of coincident sites along the line contact is consistent with a CSL boundary, the particles will form a CSL GB when their faces contact. Otherwise, when the two faces come into contact the particles may rotate about their shared ⟨100⟩ direction until the interfacial energy is sufficiently low; in principle this rotation can occur before the GB actually forms. The special feature of the first scenario is that the coincidence can be determined when the line contacts the face; no subsequent rotation about the common cube axis is then required.

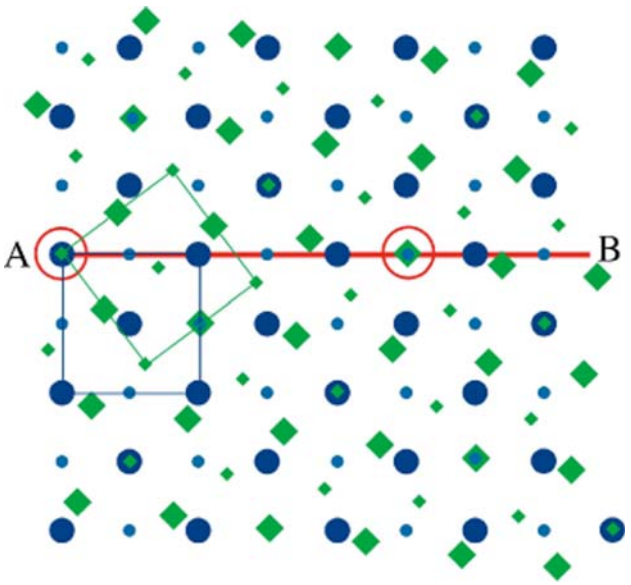

Fig. 12 CSL models for [001] $\sum = 5$ twist grain boundaries

It is emphasized that this article is not claiming that there is a relationship between $\sum$ (of the CSL or O-lattice theory) and the energy of the GB. It is also certainly not using the interfacial $\sum$ to predict GB structure. The CSL (and O-lattice) theory is a 'simple' geometric constructions and make no assumptions about energy. What this article does propose is that it instead is the geometry of the line contact that determines the preferred orientation.

The charged nature of the ions may also explain the frequency with which twist GBs are formed in which the corner of one cube is aligned with the edge of the other, as observed in the boundaries in Fig. 6b–d.

The frequency with which each CSL misorientation is observed depends on both the GB energy associated with each configuration and the kinetics of the rotation process [52]. One unique example is the $\Sigma = 17$ GB, which is predicted for MgO but rarely observed. One theory suggests that like charges of non-coincident sites may be brought too close together in this orientation, and the orientation is unfavorable because of the large ionic character of the MgO crystal [29]. It is suggested here that the contact of the line and face would be unfavorable for this orientation and thus would not occur. Smoke particles of CdO, in which the bonds exhibit a smaller ionic character (56%, compared to MgO's 73%), have been observed to form $\Sigma = 17$ GBs [29].

The fact that neither the 45° twist boundary nor the $\sum = 17$ GB are usually observed may be due to there being no line of high coincidence.

Growth boundaries

For MgO smoke particles, there is an important distinction between particles which have come into contact and particles which have grown together and are essentially one particle. This difference is especially significant in the case of the face-to-face boundaries discussed in the previous section. Though not a boundary in the traditional sense, particles are occasionally found which have either grown together or have nucleated from a common point. In this case the 'boundary' is not formed by two particles contacting in the smoke. In the example shown in Fig. 8a, the growth 'boundary' is very clear. The large particle in Fig. 8a has two elongated branches that are oriented

perpendicular to one another: the two larger particles in the image are actually one larger particle.

In Fig. 8b, the boundary is much more difficult to identify and could be mistaken for a face-to-face boundary. Careful inspection of the contrast at the cube edges indicates that neither of these two 'particles' is actually a perfect cube.

It is important to note the difference between two particles that have come into contact with each other and two particles that have joined and then grown to as one crystal, i.e., growth boundaries must be distinguished from other types of boundaries.

Conclusions

TEM samples of MgO nanocubes were produced by burning Mg metal to produce a smoke consisting of nanoscale particles of MgO. Contacting particles were found to form unique boundaries due, in part, to the low coordination of the face, edge, and corner atoms. It is proposed here that the boundaries actually form as the result of an initial point contact in the smoke followed by a line of contact. This contact line ultimately determines the type of boundary formed as the cube particles rotate to bond across a common {001} plane. Thus, for example, the $\sum = 5$ GB does not form by faces joining and the grains then rotating into a lower energy configuration, but is instead the line contact forms first and the GB is then formed ab initio in the exact (or nearly exact) $\sum = 5$ orientation; no subsequent rotation (which would require the glide of screw dislocations on the (001) plane) occurs. The formation of the low-$\sum$ GBs is not therefore a direct result of that interface having a low energy, but rather that the line contact is particularly favored and the GB has an energy which is simply less than the combined surface energies. The ideal future study would be to control the particle growth (P_{O_2}, P_{Mg}, T, substrate, etc.) and then use in situ observation with micromanipulation. Such a study is not yet possible in the TEM, but TEM is the only technique that can provide the necessary images.

Acknowledgements This research has been supported by the IGERT program of the NSF under award number DGE-0114372 and by NSF grant number CMS0322436. The authors acknowledge support from the 3M Heltzer Endowed Chair and the University of Connecticut. They would also like to thank Nicole Munoz for help with collecting the MgO smoke, Jonathan Winterstein and Dr. Ramachandran Divakar for helpful discussions, and Jessica Riesterer and Joysurya Basy for critically reading the manuscript.

References

1. Yoshimura M, Byrappa K (2008) J Mater Sci 43:2085. doi:10.1007/s10853-007-1853-x
2. Ionita P, Spafiu F, Ghica C (2008) J Mater Sci 43:6571. doi:10.1007/s10853-008-2987-1
3. Chen X, Hutchison JL, Dobson PJ, Wakefield G (2009) J Mater Sci 44:285. doi:10.1007/s10853-008-3055-6
4. Gautam ARS, Howe JM (2009) J Mater Sci 10.1007/s10853-008-3080-5
5. Carter CB, Norton MG (2007) Ceramic materials: science & engineering. Springer, New York
6. Johnson MT, Michael JR, Gilliss SR, Carter CB (1999) Philos Mag A 79:2877
7. Nakamura Y, Kudo S, Mukaida M, Ohshima S (2003) Phys C 392–396 II:1276
8. Lin C, Xu YH, Naramoto H, Wei P, Kitazawa S, Narumi K (2002) J Phys D Appl Phys 35:1864
9. Norton MG, Hellman ES, Hartford EH Jr, Carter CB (1991) J Cryst Growth 113:716
10. Zhu TJ, Lu L, Zhao XB (2006) Mater Sci Eng B 129:96
11. Ha CH, Kim JS, Jeong DC, Whang KW (2004) J Appl Phys 96:4807
12. Yoshida K, Uchiike H, Sawa M (1999) IEICE Trans Electron E82-C:1798
13. Urade T, Iemori T, Osawa M, Nakayama N, Morita I (1976) IEEE Trans Electron Dev 23:313
14. Uchiike H, Miura K, Nakayama N, Shinoda T, Fukushima Y (1976) IEEE Trans Electron Dev 23:1211
15. Wagner GW, Bartram PW, Koper O, Klabunde KJ (1999) J Phys Chem B 103:3225
16. Rajagopalan S, Koper O, Decker S, Klabunde KJ (2002) Chem Eur J 8:2602
17. Mishakov IV, Zaikovskii VI, Heroux DS, Bedilo AF, Chesnokov VV, Volodin AM, Martyanov IN, Filimonova SV, Parmon VN, Klabunde KJ (2005) J Phys Chem 109:6982
18. Leofanti G, Solari M, Tauszik GR, Garbassi F, Galvagno S, Schwank J (1982) Appl Catal 3:131
19. Hattori H (2001) Appl Catal A 222:247
20. Richards R, Mulukutla RS, Mishakov I, Chesnokov V, Volodin A, Zaikovski V, Sun N, Klabunde KJ (2001) Scr Mater 44:1663
21. Ma R, Bando Y (2003) Chem Phys Lett 370:770
22. Yang Q, Sha J, Wang L, Wang J, Yang D (2006) Mater Sci Eng C 26:1097
23. Zhao M, Chen XL, Zhang XN, Dai L, Jian JK, Xu YP (2004) Appl Phys A 79:429
24. Yang PD, Lieber CM (1996) Science 273:1836
25. Perrey CR, Carter CB (2006) J Mater Sci 41:2711. doi:10.1007/s10853-006-7874-z
26. Williams DB, Carter CB (2008) Transmission electron microscopy: a textbook for materials science. Springer, New York
27. Heidenreich RD (1942) Phys Rev 62:291
28. Chaudhari P, Matthews JW (1970) Appl Phys Lett 17:115
29. Chaudhari P, Matthews JW (1971) J Appl Phys 42:3063
30. Friedel G (1926) Leçons de Cristallographie. Berger-Levrault, Paris
31. Jones CF, Segall RL, Smart RSC, Turner PS (1980) Philos Mag A 42:267
32. Altman IS, Agranovski IE (2004) Appl Phys Lett 84:5130
33. Stankic S, Müller M, Diwald O, Sterrer M, Knözinger E, Bernardi J (2005) Angew Chem 44:4917
34. Boothroyd CB, Humphreys CJ (1993) Ultramicroscopy 52:318
35. Jones CF, Reeve RA, Rigg R, Segall RL, Smart RSC, Turner PS (1984) J Chem Soc, Faraday Trans I 80:2609
36. Winterstein JP, Carter CB (2009) Submitted
37. Thölén AR (2006) J Mater Sci 41:4466. doi:10.1007/s10853-006-0092-x
38. Thölén AR, Yao Y (2003) J Colloid Interface Sci 286:362
39. Yao Y, Thölén AR (1999) Nanostr Mater 12:661
40. Thölén AR (1990) Phase Transitions 24–26:375

41. Thölén AR (1979) Acta Metall 27:1765
42. Deneen J, Mook WM, Minor A, Gerberich WW, Carter CB (2006) J Mater Sci 41:4477. doi:10.1007/s10853-006-0085-9
43. Cosandey F, Komem Y, Bauer CL, Carter CB (1978) Scr Metall 12:577
44. Hirth JP, Lothe J (1982) Theory of dislocations. Wiley, New York
45. Goodhew PJ, Smith DA (1980) Scr Metall 14:59
46. Otsuki A (2001) Acta Mater 49:1737
47. Surholt T, Molodov DA, Herzig C (1998) Acta Mater 46:5345
48. Doni EG, Bleris GL (1990) Scr Metall Mater 24:1991
49. Mykura H, Bansal PS, Lewis MH (1980) Philos Mag A 42:225
50. Saylor DM, Morawiec A, Adams BL, Rohrer GS (2000) Interface Sci 8:131
51. Saylor DM, Morawiec A, Rohrer GS (2003) Acta Mater 51:3663
52. Pond RC, Smith DA (1977) Scr Metall 11:77